10-24-2011

Nonlinear parametric amplification and attenuation in a base-excited cantilever beam

Vijay Kumar
Purdue University, kumar2@purdue.edu

Jacob K. Miller
Purdue University, jacobmiller@purdue.edu

Jeffrey F. Rhoads
Purdue University, jfrhoads@purdue.edu

Kumar, Vijay; Miller, Jacob K.; and Rhoads, Jeffrey F., "Nonlinear parametric amplification and attenuation in a base-excited cantilever beam" (2011). *Birck and NCN Publications.* Paper 777.
http://dx.doi.org/10.1016/j.jsv.2011.06.006

Journal of Sound and Vibration 330 (2011) 5401–5409

Contents lists available at ScienceDirect

Journal of Sound and Vibration

journal homepage: www.elsevier.com/locate/jsvi

Nonlinear parametric amplification and attenuation in a base-excited cantilever beam

Vijay Kumar, Jacob K. Miller, Jeffrey F. Rhoads *

School of Mechanical Engineering, Ray W. Herrick Laboratories, and Birck Nanotechnology Center, Purdue University, West Lafayette, IN 47907, United States

ARTICLE INFO

Article history:
Received 5 January 2011
Received in revised form
8 June 2011
Accepted 9 June 2011
Handling Editor: L.N. Virgin
Available online 28 June 2011

ABSTRACT

This work investigates the nonlinear behavior of a representative parametrically amplified macroscale structure. Specifically, the effort examines the effects of structural and inertial nonlinearities on the near-resonant response of a base-excited, flexible cantilever beam driven by a combined (simultaneously parametric and direct) excitation. The prototypical structure is modeled using classical energy methods and key response metrics are analyzed through the use of the method of averaging. A series of experimental investigations are performed to validate analytically predicted behaviors. The work demonstrates that with the proper selection of various system parameters, both vibration amplification and attenuation can be efficiently achieved. This work provides a baseline understanding of the effect of nonlinearities on parametrically excited systems and is expected to guide future work on micro/nanoscale systems, where parametric excitations arise quite naturally.

1. Introduction

In mechanical and electromechanical contexts, parametric amplification refers to the process of driving a system into sustained, near-resonant oscillation (through a direct excitation) and subsequently manipulating the amplitude of this oscillation through the variation of an energy storage element, such as a capacitor, inductor, or spring (a parametric excitation). Though this concept has been successfully employed for decades in electrical systems, such as power and communication systems and Josephson junctions [1,2], parametric amplification has only recently garnered significant attention from the mechanical systems community, specifically in the area of micro/nanoelectromechanical systems (MEMS and NEMS). A representative early effort in this area was conducted by Rugar and Grütter, who explored resonant amplification in a microcantilever simultaneously actuated by piezoelectric and electrostatic elements [3]. Subsequent to this work, a number of studies have explored parametric amplification in the context of torsional microresonators [4,5], coupled microresonators [6], microbeams [7–9], and, recently, resonant nanosystems [10].

While a considerable amount of attention has focused on the modeling, analysis, and implementation of parametric amplification in micro/nanoscale mechanical systems, comparatively few studies have investigated the phenomenon at the macroscale, where an appreciable number of applications potentially exist. In prior work, Rhoads et al. investigated linear parametric amplification in a macroscale cantilever beam driven by longitudinal and transverse base excitations [11]. This work reported near-resonant amplifier gains of 1.4–1.6 and showed that with careful selection of system parameters, vibrations could also be suppressed. Ecker, Kim, and their respective collaborators have investigated related

* Corresponding author.
E-mail addresses: kumar2@purdue.edu (V. Kumar), mille411@purdue.edu (J.K. Miller), jfrhoads@purdue.edu (J.F. Rhoads).

0022-460X/$ - see front matter © 2011 Elsevier Ltd. All rights reserved.
doi:10.1016/j.jsv.2011.06.006

dynamic phenomenon in many of their respective works (see, for example, [12,13]). The effect of nonlinearity on a parametric amplifier was recently analyzed by Rhoads and Shaw [14,15]. These studies showed that while nonlinearities limit the gains that can be realized using a parametric amplifier, they do not explicitly prohibit low-noise signal amplification. Leveraging, in part, the results of this work, Nichol et al. recently utilized active nonlinear feedback to control the near-resonant response of a silicon nanowire resonator exhibiting a distinctly nonlinear frequency response structure [10].

In this paper, the nonlinear behavior of a macroscale, base-excited cantilever beam driven by both direct and degenerate parametric excitations is investigated. A cantilever beam with longitudinal and transverse base excitations is modeled using classical energy methods and subsequently analyzed via the method of averaging to recover key amplifier metrics. A simple experimental investigation is then used to validate analytically predicted behaviors and, ultimately, to develop an improved understanding of nonlinear parametric amplification and attenuation.

2. Modeling

The system of interest here is a cantilever beam simultaneously actuated by longitudinal and transverse base excitations, see Fig. 1. The equation of motion governing the transverse vibrations of this system can be derived using energy methods, as detailed in [11,16]. For a uniform beam undergoing deflections of $u(s,t)$ and $v(s,t)$ in the x and y directions, respectively, the kinematic constraint relating the local deflection angle ψ to the displacements u and v is given by

$$\tan\psi = \frac{v'}{1+u'}, \tag{1}$$

where u, v and ψ are defined as in Fig. 1 and $(\bullet)'$ represents a spatial derivative operator referenced to the arc length variable s. Assuming that the beam has negligible rotational inertia and defining the temporal derivatives with respect to the time variable t as $\dot{(\bullet)}$, the specific Lagrangian associated with the system of interest can be written as

$$\bar{L} = \tfrac{1}{2}\rho A[(\dot{u}+\dot{u}_p)^2+(\dot{v}+\dot{v}_p)^2] - \tfrac{1}{2}EI(\psi')^2, \tag{2}$$

where u_p and v_p specify the base motions in the longitudinal and transverse directions and ρ, A, E, and I represent the beam's mass density, cross-sectional area, elastic modulus, and area moment of inertia. Constraining the neutral axis of the beam to be inextensible and applying extended Hamilton's principle results in a variational equation for the system, given by

$$\delta H = \delta\int_{t_1}^{t_2}\int_0^l \left[\bar{L}+\frac{1}{2}\lambda[1-(1+u')^2-(v')^2]\right]\mathrm{d}s\,\mathrm{d}t + \int_{t_1}^{t_2}\int_0^l (Q_u\delta u + Q_v\delta v)\,\mathrm{d}s\,\mathrm{d}t = 0, \tag{3}$$

where l represents the length of the beam, λ is the Lagrange multiplier utilized to maintain the inextensibility constraint, and Q_u and Q_v represent the generalized forces not explicitly accounted for in the previously defined Lagrangian. For the system of interest, the generalized forces can be approximated as

$$Q_u = -\rho A g, \quad Q_v = -c\dot{v}, \tag{4}$$

where g represents the acceleration due to gravity and c represents a specific viscous damping coefficient. Substituting Eqs. (2) and (4) into Eq. (3) and solving with Eq. (1) yields a pair of coupled equations governing the motion of the system. The equation

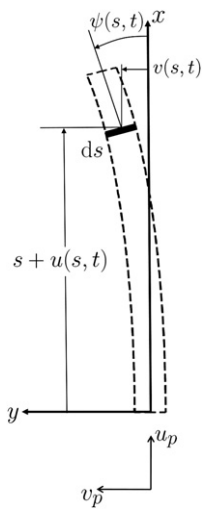

Fig. 1. Schematic of the base-excited cantilever beam considered in this work.

governing the transverse dynamics of the system can be recovered from this set by solving for the Lagrange multiplier in the equation governing longitudinal motion and substituting the result into the remaining equation. Employing Taylor series expansions where prudent and truncating the result to retain up to third-order terms yields a model given by

$$\rho A\ddot{v}+c\dot{v}+EI[v^{iv}+(v'')^3+4v'v''v'''+(v')^2v^{iv}]+\frac{1}{2}\rho Av''\int_l^s\frac{\partial^2}{\partial t^2}\int_0^s(v')^2\,\mathrm{d}s\,\mathrm{d}s$$
$$+\frac{1}{2}\rho Av'\frac{\partial^2}{\partial t^2}\int_0^s(v')^2\,\mathrm{d}s-\rho Av''\int_l^s(\ddot{u}_p+g)\,\mathrm{d}s-\rho Av'(\ddot{u}_p+g)-\frac{1}{2}\rho A(v')^3(\ddot{u}_p+g)$$
$$-\frac{3}{2}\rho A(v')^2(v'')\int_l^s(\ddot{u}_p+g)\,\mathrm{d}s=-\rho A\ddot{v}_p. \tag{5}$$

Nondimensionalizing the above equation by scaling the arc length variable with respect to the length of the beam, the beam displacements with respect to a characteristic length v_0, and the time variable with respect to a characteristic period T of the system, according to

$$\hat{s}=\frac{s}{l},\quad \hat{v}=\frac{v}{v_0},\quad \hat{u}_p=\frac{u_p}{v_0},\quad \hat{v}_p=\frac{v_p}{v_0},\quad \hat{t}=\frac{t}{T}, \tag{6}$$

where

$$T=\sqrt{\frac{\rho Al^4}{EI}},$$

results in the final distributed-parameter model of the system:

$$\ddot{\hat{v}}+\hat{c}\dot{\hat{v}}+\hat{v}^{iv}-\frac{v_0}{l}\hat{v}''\int_1^{\hat{s}}\ddot{\hat{u}}_p\,\mathrm{d}\hat{s}-\frac{\rho Al^3g}{EI}(\hat{s}-1)\hat{v}''-\frac{v_0}{l}\hat{v}'\ddot{\hat{u}}_p-\frac{\rho Al^3g}{EI}\hat{v}'+\frac{v_0^2}{l^2}(\hat{v}'')^3+\frac{4v_0^2}{l^2}\hat{v}'\hat{v}''\hat{v}'''+\frac{v_0^2}{l^2}(\hat{v}')^2\hat{v}^{iv}$$
$$-\frac{v_0^3}{2l^3}(\hat{v}')^3\ddot{\hat{u}}_p-\frac{\rho Av_0^2lg}{2EI}(\hat{v}')^3-\frac{3v_0^3}{2l^3}(\hat{v}')^2\hat{v}''\int_1^{\hat{s}}\ddot{\hat{u}}_p\,\mathrm{d}\hat{s}-\frac{3\rho Alv_0^2g}{2EI}(\hat{v}')^2\hat{v}''(\hat{s}-1)+\frac{v_0^2}{2l^2}\hat{v}''\int_1^{\hat{s}}\frac{\partial^2}{\partial\hat{t}^2}\int_0^{\hat{s}}(\hat{v}')^2\,\mathrm{d}\hat{s}\,\mathrm{d}\hat{s}$$
$$+\frac{v_0^2}{2l^2}\hat{v}'\frac{\partial^2}{\partial\hat{t}^2}\left[\int_0^{\hat{s}}(\hat{v}')^2\,\mathrm{d}\hat{s}\right]=-\ddot{\hat{v}}_p. \tag{7}$$

Table 1
Nondimensional parameters utilized in Eq. (12).

$z=w$
$\tau=\omega_0\hat{t},\quad (\dot{\bullet})=\frac{\mathrm{d}(\bullet)}{\mathrm{d}\tau}$
$\hat{\omega}=\omega T,\quad \Omega=\frac{\hat{\omega}}{\omega_0}$
$\omega_0^2=\int_0^1\Phi\Phi^{iv}\,\mathrm{d}\hat{s}-\frac{\rho Al^3g}{EI}\left[\int_0^1\Phi\Phi''(\hat{s}-1)\,\mathrm{d}\hat{s}+\int_0^1\Phi\Phi'\,\mathrm{d}\hat{s}\right]$
$\varepsilon\zeta=\frac{\hat{c}}{2\omega_0}$
$\varepsilon\lambda_1=\frac{\hat{A}v_0\sin\alpha}{l}\left[\int_0^1\Phi\Phi''(\hat{s}-1)\,\mathrm{d}\hat{s}+\int_0^1\Phi\Phi'\,\mathrm{d}\hat{s}\right]$
$\varepsilon\lambda_2=\frac{4\hat{B}v_0\sin\alpha}{l}\left[\int_0^1\Phi\Phi''(\hat{s}-1)\,\mathrm{d}\hat{s}+\int_0^1\Phi\Phi'\,\mathrm{d}\hat{s}\right]$
$\varepsilon\omega_0^2k_3=\frac{v_0^2}{l^2}\left[\int_0^1\Phi(\Phi'')^3\,\mathrm{d}\hat{s}+4\int_0^1\Phi\Phi'\Phi''\Phi'''\,\mathrm{d}\hat{s}+\int_0^1\Phi(\Phi')^2\Phi^{iv}\,\mathrm{d}\hat{s}\right]-\frac{3\rho Alv_0^2g}{2EI}\int_0^1\Phi(\Phi')^2\Phi''(\hat{s}-1)\,\mathrm{d}\hat{s}-\frac{\rho Av_0^2lg}{2EI}\int_0^1\Phi(\Phi')^3\,\mathrm{d}\hat{s}$
$\varepsilon\gamma_1=\frac{\hat{A}\sin\alpha v_0^3}{2l^3}\left[\int_0^1\Phi(\Phi')^3\,\mathrm{d}\hat{s}+3\int_0^1\Phi(\Phi')^2\Phi''(\hat{s}-1)\,\mathrm{d}\hat{s}\right]$
$\varepsilon\gamma_2=\frac{4\hat{B}\sin\alpha v_0^3}{2l^3}\left[\int_0^1\Phi(\Phi')^3\,\mathrm{d}\hat{s}+3\int_0^1\Phi(\Phi')^2\Phi''(\hat{s}-1)\,\mathrm{d}\hat{s}\right]$
$\varepsilon\alpha_n=\frac{v_0^2}{l^2}\left[\int_0^1\Phi\Phi''\int_1^{\hat{s}}\int_0^{\hat{s}}(\Phi')^2\,\mathrm{d}\hat{s}\,\mathrm{d}\hat{s}\,\mathrm{d}\hat{s}+\int_0^1\Phi\Phi'\int_0^{\hat{s}}(\Phi')^2\,\mathrm{d}\hat{s}\,\mathrm{d}\hat{s}\right]$
$\varepsilon\eta_1=\hat{A}\cos\alpha\int_0^1\Phi\,\mathrm{d}\hat{s},\quad \varepsilon\eta_2=4\hat{B}\cos\alpha\int_0^1\Phi\,\mathrm{d}\hat{s}$

Here,

$$\hat{c} = \frac{cT}{\rho A}. \tag{8}$$

Decomposing the displacement variable $\hat{v}$ into its spatial and temporal components according to

$$\hat{v} = w(\hat{t})\Phi(\hat{s}), \tag{9}$$

and projecting the result onto the beam's first mode shape, while simultaneously imposing that the base motions result from a unidirectional base excitation $\hat{x}_p$, given by

$$\hat{x}_p = \hat{A}\cos(\omega t+\phi)+\hat{B}\cos(2\omega t) = \hat{A}\cos(\hat{\omega}\hat{t}+\phi)+\hat{B}\cos(2\hat{\omega}\hat{t}), \tag{10}$$

and

$$\hat{u}_p = \hat{x}_p\sin\alpha, \quad \hat{v}_p = \hat{x}_p\cos\alpha, \tag{11}$$

results in the final governing equation of motion for the system:

$$\begin{aligned}\ddot{z}+2\varepsilon\zeta\dot{z}+z+[\varepsilon\lambda_1\Omega^2\cos(\Omega\tau+\phi)+\varepsilon\lambda_2\Omega^2\cos(2\Omega\tau)]z+\varepsilon k_3 z^3+[\varepsilon\gamma_1\Omega^2\cos(\Omega\tau+\phi)+\varepsilon\gamma_2\Omega^2\cos(2\Omega\tau)]z^3\\ +\varepsilon\alpha_n(z\dot{z}^2+z^2\ddot{z}) = \varepsilon\eta_1\Omega^2\cos(\Omega\tau+\phi)+\varepsilon\eta_2\Omega^2\cos(2\Omega\tau).\end{aligned} \tag{12}$$

The nondimensional parameters included here are defined in Table 1. Note that ε is a small bookkeeping parameter introduced to facilitate analysis. Also note that the derivative operator $(\dot{\bullet})$ has been redefined.

3. Analysis

Since Eq. (12) lacks a tractable closed-form solution, the system is analyzed using the method of averaging. To this end, a constrained coordinate transformation of the form

$$z(\tau) = X(\tau)\cos(\Omega\tau)+Y(\tau)\sin(\Omega\tau), \quad z'(\tau) = -X(\tau)\Omega\sin(\Omega\tau)+Y(\tau)\Omega\cos(\Omega\tau), \tag{13}$$

as well as a detuning parameter σ, defined according to

$$\sigma = \frac{\Omega-1}{\varepsilon}, \tag{14}$$

is introduced into Eq. (12). Substituting Eqs. (13) and (14) into Eq. (12), isolating dynamic variables, and integrating the result over a period of oscillation $(2\pi/\Omega)$ yields the system's averaged equations, which are given by

$$\begin{aligned}X' &= -\tfrac{1}{8}\varepsilon[8\zeta X+(8\sigma+2\lambda_2)Y-(3k_3-2\alpha_n)(X^2+Y^2)Y+2\gamma_2 Y^3-4\eta_1\sin\phi]+\mathcal{O}(\varepsilon^2),\\ Y' &= -\tfrac{1}{8}\varepsilon[8\zeta Y+(2\lambda_2-8\sigma)X+(3k_3-2\alpha_n)(X^2+Y^2)X+2\gamma_2 X^3-4\eta_1\cos\phi]+\mathcal{O}(\varepsilon^2).\end{aligned} \tag{15}$$

Note that by using the method of averaging, the non-autonomous, second-order nonlinear differential equation governing the system's behavior has been transformed into a pair of autonomous, first-order differential equations. It can be observed in the averaged equations that the terms with coefficients η_2, λ_1, and γ_1 do not appear and hence, do not affect the steady-state response of the system in a meaningful way. This can be attributed to the fact that these terms correspond to the non-resonant components in the equation of motion. Furthermore, by evaluating the coefficients of the averaged equations, it can be seen that for the system under consideration here, the value of γ_2 is at least two orders of magnitude smaller than comparable terms, and is thus ignored throughout the remainder of the work. Finally, to facilitate analysis, the cubic stiffness term and the inertial nonlinearity coefficient are joined together into a single effective nonlinear coefficient, $N_{eff} = 3k_3-2\alpha_n$.

The steady-state solutions associated with the averaged equations detailed above can be acquired by setting $(X',Y') = (0,0)$ and solving for X and Y. Using these values of X and Y, the steady-state amplitude and phase of each solution can be obtained through a direct Cartesian to polar coordinate change.

For reference purposes, the frequency response of the system has been investigated by benchmarking pertinent excitation parameters against the classical parametric instability threshold (Arnold tongue), see Fig. 2. Fig. 3(a) and (b) highlight the frequency response of the system at various pump amplitudes for $\phi = 90^\circ$. It can be seen that at pump amplitudes less than the threshold value, for most positive values of N_{eff} (i.e. those where nonlinear parametric effects are negligible), the system exhibits a Duffing-like hardening response (Fig. 3(a)). As the pump value is increased above the linear parametric instability threshold, the response bifurcates yielding two coexisting resonances, one, loosely speaking, attributable to the direct excitation and another attributable to the parametric excitation (Fig. 3(b)). It is important to note, as noted in [14,15], that the upper solution branch remains qualitatively unchanged in each of the above cases, and thus, provided operation on the upper response branch, the coexistence of multiple stable steady-state solutions presents minimal complication in the context of parametric amplification.

Fig. 3(c) and (d) highlight the frequency response of the system at various pump amplitudes for $\phi = 10^\circ$. It can be seen that at pump amplitudes less than the threshold value, there is a slight decrease in the peak amplitude of the system, or in other words, parametric attenuation (Fig. 3(c)). This effect can be enhanced with proper parameter selection/system design. As the pump value is increased above the linear parametric instability threshold, the response bifurcates yielding

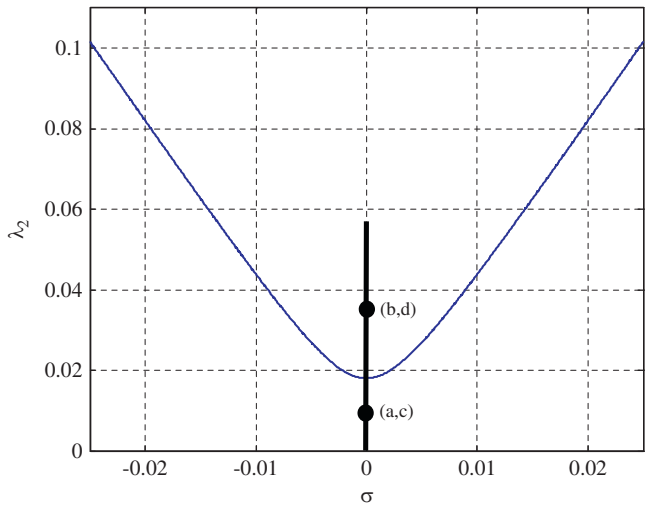

Fig. 2. Instability threshold (Arnold tongue) corresponding to the onset of linear parametric resonance. In the system of interest, this boundary dictates the existence of additional solution branches in the resonator's steady-state frequency response structure, as highlighted in Fig. 3. Note that, here and in Figs. 3 and 4, the assumed value of the system's damping ratio is $\zeta = 0.0045$, unless otherwise stated.

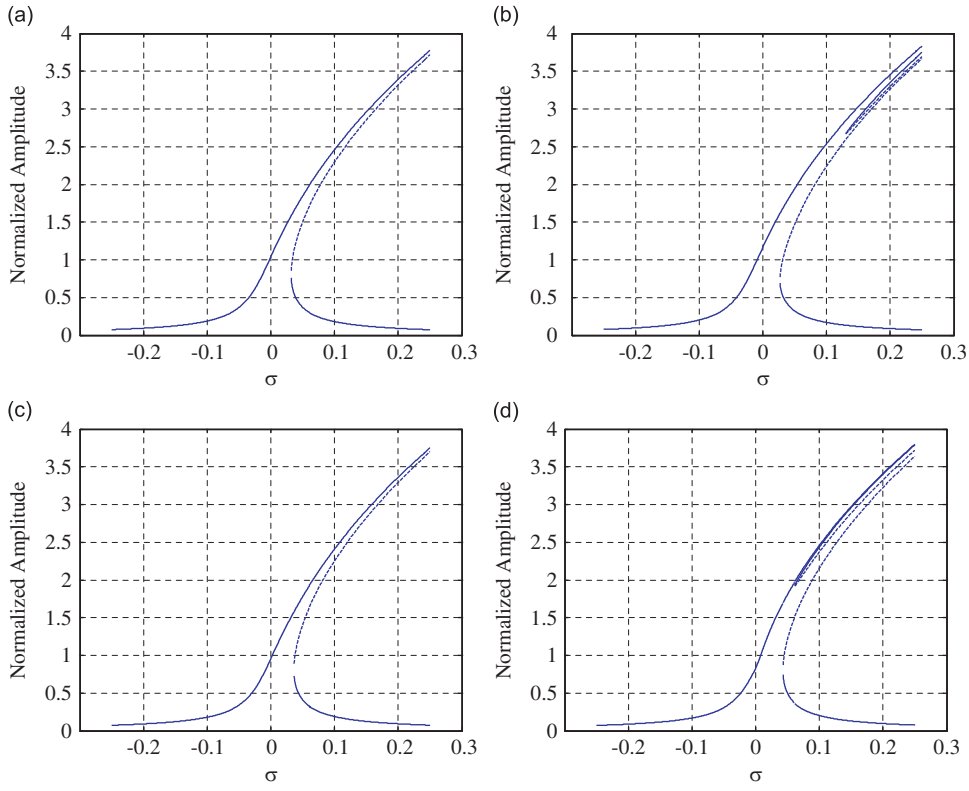

Fig. 3. Theoretical frequency response of the system driven (a) with a pump amplitude below the linear parametric instability threshold (for $\phi = 90^\circ$), (b) with a pump amplitude far above the instability threshold (for $\phi = 90^\circ$), (c) with a pump amplitude below the linear parametric instability threshold (for $\phi = 10^\circ$) and (d) with a pump amplitude far above the instability threshold (for $\phi = 10^\circ$). (a) and (c) represent instances in which the ratio of the pump amplitude to the critical pump amplitude as determined by the linear instability threshold is 0.5. Likewise, (b) and (d) represent instances in which the ratio of pump amplitude to the critical pump amplitude as determined by the linear instability threshold is 2. Note that the solid lines represent stable steady-state solutions, while the dotted lines represent unstable solutions. To generate all the above plots, the direct excitation amplitude is chosen as $\hat{A} = 1$. Also note that the normalized amplitude is defined to be the ratio of the output amplitude at any particular frequency to the output amplitude of unpumped case at resonance.

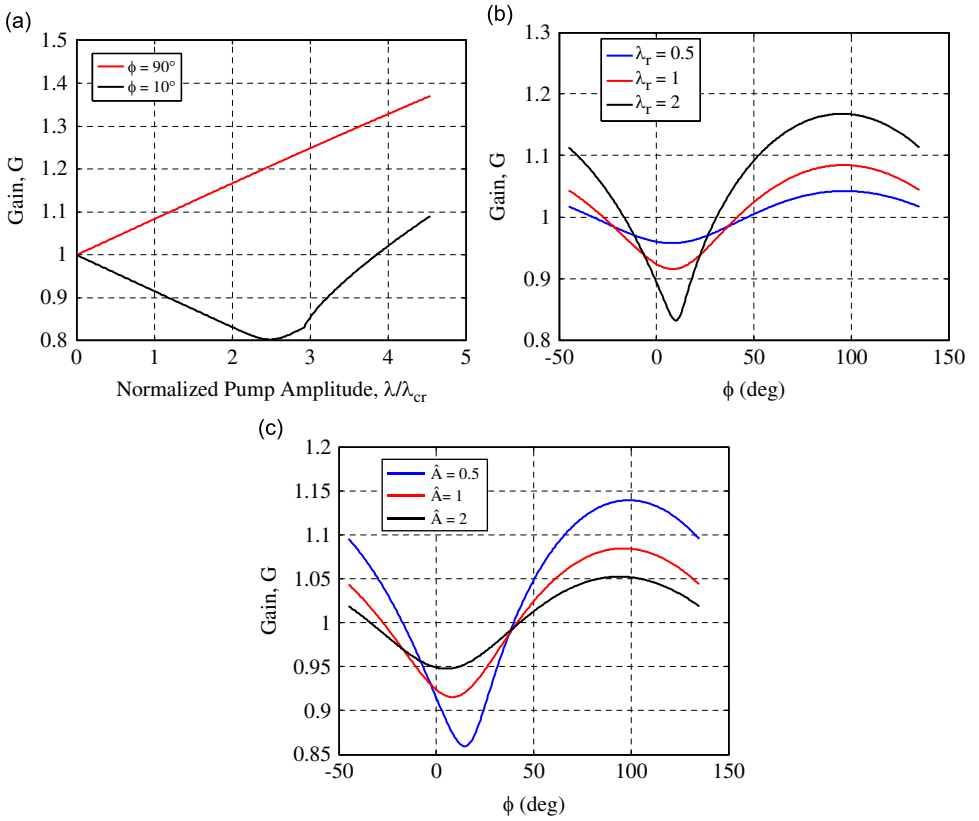

Fig. 4. (a) Gain of the amplifier, $G(\sigma=0)$, plotted against the normalized pump amplitude for different values of ϕ. Note that the pump amplitude has been normalized with respect to the critical threshold value associated with the onset of linear parametric resonance and the direct excitation amplitude is chosen as $\hat{A}=1$. (b) Gain of the amplifier plotted against the relative phase angle between the direct excitation and parametric pump, ϕ, for different values of λ_r, the ratio of parametric pump and the aforementioned critical pump amplitude. Note that the direct excitation amplitude is maintained constant ($\hat{A}=1$) for all the three cases. (c) Gain of the amplifier plotted against the relative phase angle between the direct excitation and parametric pump, ϕ, for different values of $\hat{A}$, the direct excitation amplitude. Note that λ_r is maintained constant ($\lambda_r=1$) for all the three cases.

two coexisting resonances, one, loosely speaking, attributable to the direct excitation and another attributable to the parametric excitation (Fig. 3(d)). It is important to note, for values of pump amplitude higher than the critical pump value, the system response is qualitatively similar to the response when $\phi=90^\circ$. Therefore, parametric attenuation is effective only in a limited range of pump amplitudes, as determined by the linear instability threshold, relative phase of the excitation, and strength of the nonlinearity.

The performance of a parametric amplifier is commonly quantified through a gain metric given by

$$G(\sigma=0)=\frac{a}{a|_{\lambda_2=0}}, \tag{16}$$

where a is the resonant amplitude of the system's upper frequency response branch in the presence of a parametric pump signal and $a|_{\lambda_2=0}$ is the resonant amplitude of the system's upper frequency response branch in the absence of the aforementioned pump. Fig. 4(a) highlights the gain versus pump amplitude behavior of a representative system for different values of the relative phase angle ϕ. Note that the pump amplitude is normalized with respect to the pump value corresponding to the onset of linear parametric resonance. As evident from the figure, for relative phase angles near 90°, the system gain monotonically increases with parametric pump amplitude, even beyond the threshold pump amplitude associated with the onset of linear parametric resonance. Accordingly, parametric amplifiers can be operated above this traditional operating threshold and used to realize meaningful gains, even in the presence of non-trivial system nonlinearities. For relative phase angles near 10°, the amplifier gain decreases well below unity with increasing pump amplitude, and then increases following the onset of linear parametric resonance. This response feature facilitates vibration attenuation.

Fig. 4(b) and (c) highlight the phase dependence of a representative parametric amplifier's gain as a function of parametric pump amplitude and the direct excitation amplitude, respectively. As evident, the system features parameter windows of both amplification and attenuation, which vary strongly with pump and the direct excitation amplitudes (as well as nonlinearity). It should be noted that the presence of a nonlinearity in the system also induces an asymmetry in the

phase-gain relationship resulting in a modification of the operating conditions corresponding to maximum amplification and attenuation, which have been identified in prior literature (see, for example, [3,11]).

4. Experimental investigation

To validate the analytical observations detailed in the preceding section and [14,15], a simple experiment was conducted. As highlighted in Figs. 5 and 6, the experimental apparatus consisted of a base-excited cantilever beam, electrodynamic shaker, and accompanying electronics. To excite the system, a signal was digitally constructed in LabVIEW software and physically realized via a multi-channel arbitrary waveform generator (Fluke 294). Two channels of the waveform generator were locked in a 1:2 frequency ratio and the output of both the channels were electronically summed. This signal was then routed to a TIRA BAA 500 power amplifier and, in turn, a TIRA 5514 electrodynamic shaker. A cantilevered spring steel beam (131.3 mm $\times$ 19.1 mm $\times$ 0.58 mm, with first natural frequency $f_1 \approx 22.14$ Hz) was mounted to this shaker at a 10° offset from the vertical to facilitate both direct and parametric excitations. A single-axis accelerometer (Crossbow CXL04GP1Z) was used to capture the induced shaker vibration in order to study the relationship between the input signal to the shaker and the shaker's vibration. The transverse vibration of the cantilever beam was measured using a pair of strain gauges (placed on either side of the beam and connected in a half-bridge configuration) and a signal conditioning amplifier (Vishay 2310B). The output from the accelerometer and from the strain gauges were recorded using a data acquisition system (Agilent U2718) and LabVIEW software.

The system's damping ratio was recovered using logarithmic decrement methods ($\varepsilon\zeta = 0.0045$). To study the frequency response of the system, the steady-state response amplitude was analyzed at representative phase angles and different pump values. Specifically, the response of the system was acquired by holding the direct excitation and the phase constant, while increasing the locked excitation frequencies.

Fig. 7(a) shows the experimental frequency response of the system obtained by sweeping the excitation frequency up for pump values which are 0, 33 and 99 percent of the critical pump amplitude corresponding to the onset of parametric resonance. It should be noted that the pump values reported here have been normalized with respect to the experimentally recovered critical pump amplitude. As evident, the system becomes increasingly nonlinear as the

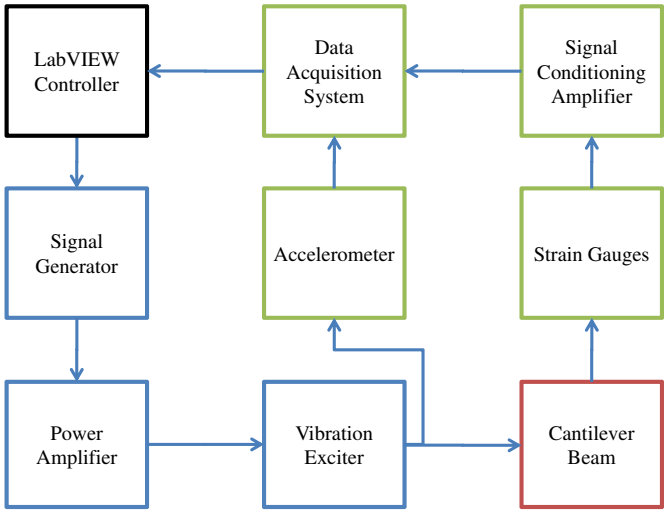

Fig. 5. Block diagram of the experimental setup.

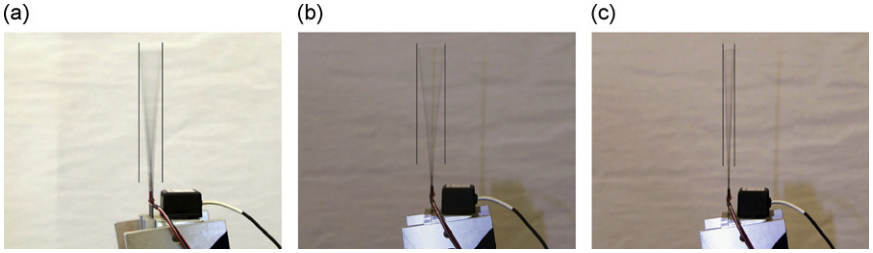

Fig. 6. The cantilever beam driven at resonance (a) without a parametric pump, (b) with an amplifying parametric pump, and (c) with an attenuating parametric pump.

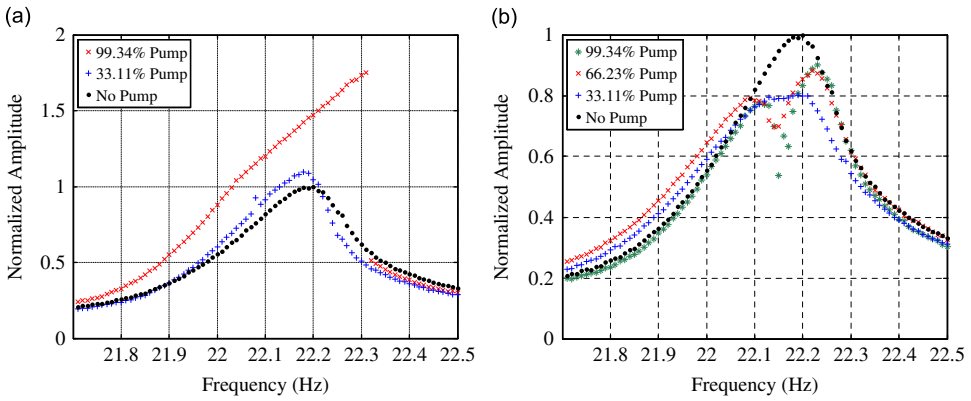

Fig. 7. Experimental frequency response of the system, obtained via an up sweep, for relative phase values of (a) $\phi = 90^\circ$ and (b) $\phi = 0^\circ$. Note that the amplitude is normalized such that the peak amplitude for the unpumped case is unity.

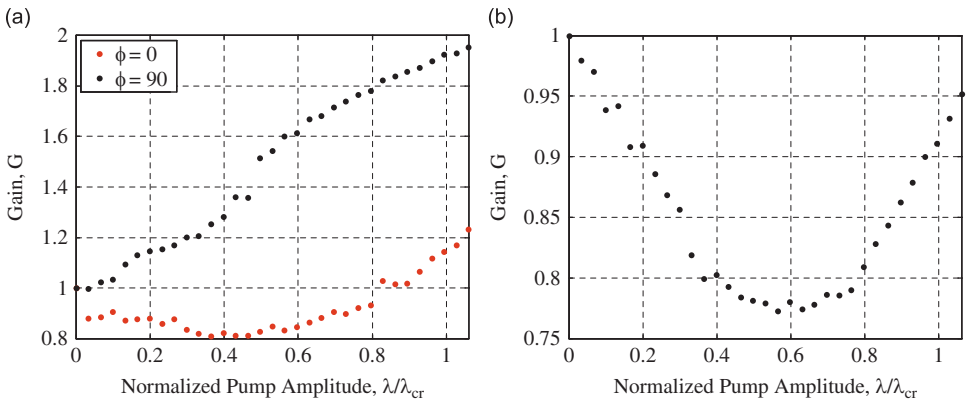

Fig. 8. Experimentally obtained amplifier gain plotted as a function of normalized pump amplitude for (a) $\phi = 90^\circ$ and 0° at resonance and (b) $\phi = 0^\circ$ at anti-resonance. Note that the pump amplitude is normalized against the experimentally obtained threshold value. Also note that the normalized amplitude is the ratio of the output amplitude at any particular frequency to the output amplitude of unpumped case at resonance.

amplitude of vibration increases. At lower pump amplitudes (0 and 33 percent), the system shows a near-linear response, but as the pump amplitude is further increased and higher gains are recovered, the nonlinearity in the system plays a major part in shaping the frequency response of the system.

Fig. 7(b) shows the response of the system obtained by sweeping the excitation frequency (up) for normalized pump amplitude values of 0, 33, 66 and 99 percent at a phase angle of $\phi = 0$, for the same value of ($\hat{A}$) utilized in Fig. 7(a). The frequency response of the system for this set of conditions is notable. As predicted by theory, there is a marked decrease in the peak amplitude of the system as the pump amplitude is initially increased. This is accompanied by a dip in the frequency response slightly away from resonance. As previously noted, because of this feature, parametric pumping can be used for vibration attenuation as well.

Fig. 8(a) highlights the relationship between amplifier gain and normalized pump amplitude, at resonance, for phase angles of $\phi = 90^\circ$ and 0°. The model appears to correlate well with the experimental results. Gains approaching 1.9 can be realized before the pump threshold is reached for $\phi = 90^\circ$ and the gain continues to increase as the pump amplitude is further increased. For $\phi = 0^\circ$, the vibration is attenuated considerably, with gains initially decreasing and then increasing again near the onset of parametric resonance. Fig. 8(b) shows the relationship between amplifier gain and normalized pump amplitude for a phase angle of $\phi = 0^\circ$, measured at the "anti-resonance" in the system's frequency response. It can be seen that there is a much higher attenuation at this operating point, as compared to resonant operation. By appropriately tracking this frequency, maximum attenuation can be realized.

As previously noted, the system response is a strong function of the relative phase angle (ϕ) between the direct excitation signal and the parametric pump. Fig. 9(a) and (b) shows the response of the system for various values of ϕ at pump amplitudes 33 and 66 percent of the critical pump amplitude, measured at resonance. It can be seen that as the phase angle changes, the gain of the system varies periodically with maximum attenuation observed at a phase angle close to 40° and maximum amplification occurring near a phase angle of 90°.

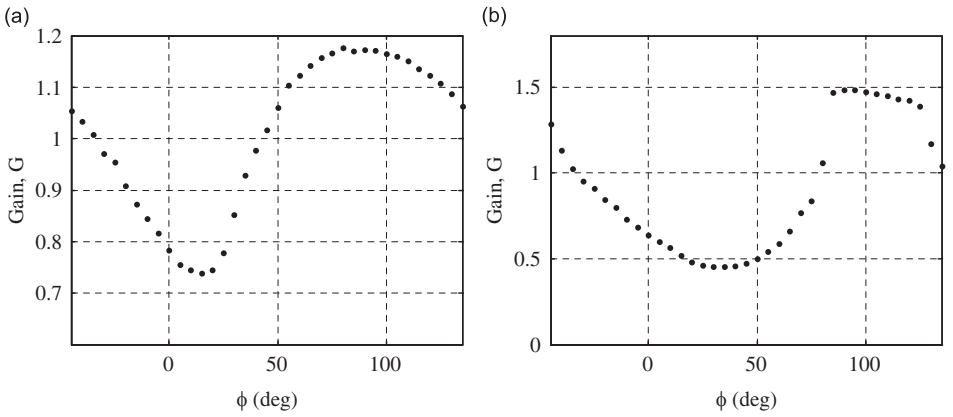

Fig. 9. Gain/phase relationship for pump amplitudes: (a) 33 percent of the critical pump amplitude and (b) 66 percent of the critical pump amplitude.

5. Conclusion

This work investigated the effects of structural and inertial nonlinearities on the near-resonant response of a base-excited, flexible cantilever beam driven by a combined (simultaneously parametric and direct) excitation. The structure was modeled using classical energy methods and key response metrics were recovered through the use of the method of averaging. A series of experimental investigations were performed to validate analytically predicted behaviors. The work demonstrated that with the proper selection of various system parameters, both vibration amplification and attenuation can be efficiently achieved. The results detailed herein provide a baseline understanding of the effect of nonlinearities on parametrically excited systems, explaining the anomalous behavior reported in [9] and is guiding ongoing work at the micro- and nanoscales.

Acknowledgment

This work was partially supported by the National Science Foundation under Grant 0826276. Student support was graciously provided by Purdue University and the Purdue Research Foundation.

References

[1] W.W. Mumford, Some notes on the history of parametric transducers, *Proceedings of the IRE* 48 (5) (1960) 848–853.
[2] W.H. Louisell, *Coupled Mode and Parametric Electronics*, John Wiley & Sons, New York, 1960.
[3] D. Rugar, P. Grutter, Mechanical parametric amplification and thermomechanical noise squeezing, *Physical Review Letters* 67 (6) (1991) 699–702.
[4] D.W. Carr, S. Evoy, L. Sekaric, H.G. Craighead, J.M. Parpia, Parametric amplification in a torsional microresonator, *Applied Physics Letters* 77 (10) (2000) 1545–1547.
[5] R. Baskaran, K.L. Turner, Mechanical domain coupled mode parametric resonance and amplification in a torsional mode micro electro mechanical oscillator, *Journal of Micromechanics and Microengineering* 13 (5) (2003) 701–707.
[6] A. Olkhovets, D.W. Carr, J.M. Parpia, H.G. Craighead, Non-degenerate nanomechanical parametric amplifier, in: *Proceedings of MEMS 2001: The 14th IEEE International Conference on Micro Electro Mechanical Systems*, Interlaken, Switzerland 2001, pp. 298–300.
[7] T. Ono, H. Wakamatsu, M. Esashi, Parametrically amplified thermal resonant sensor with pseudo-cooling effect, *Journal of Micromechanics and Microengineering* 15 (12) (2005) 2282–2288.
[8] A. Dana, F. Ho, Y. Yamamoto, Mechanical parametric amplification in piezoresistive gallium arsenide microcantilevers, *Applied Physics Letters* 72 (10) (1998) 1152–1154.
[9] I. Mahboob, H. Yamaguchi, Piezoelectrically pumped parametric amplification and Q enhancement in an electromechanical oscillator, *Applied Physics Letters* 92 (2008) 173109.
[10] J.M. Nichol, E.R. Hemesath, L.J. Lauhon, R. Budakian, Controlling the nonlinearity of silicon nanowire resonators using active feedback, *Applied Physics Letters* 95 (2009) 123116.
[11] J.F. Rhoads, N.J. Miller, S.W. Shaw, B.F. Feeny, Mechanical domain parametric amplification, *Journal of Vibration and Acoustics* 130 (2008) 061006.
[12] H. Ecker, Exploring the use of parametric excitation, in: *Proceedings of RASD 2010: The 10th International Conference on Recent Advances in Structural Dynamics*, Southampton, United Kingdom, 2010.
[13] C.H. Kim, C.-W. Lee, N.C. Perkins, Nonlinear vibration of sheet metal under interacting parametric and external excitation during manufacturing, *Journal of Vibration and Acoustics* 127 (1) (2005) 36–43.
[14] J.F. Rhoads, S.W. Shaw, The effects of nonlinearity on parametric amplifiers, in: *Proceedings of IDETC/CIE 2008: The ASME 2008 International Design Engineering Technical Conferences and Computers and Information in Engineering Conference, Second International Conference on Micro- and Nanosystems*, Brooklyn, New York, 2008 (DETC2008-49594).
[15] J.F. Rhoads, S.W. Shaw, The impact of nonlinearity on degenerate parametric amplifiers, *Applied Physics Letters* 96 (2010) 234101.
[16] M.R.M. Crespo da Silva, C.C. Glynn, Nonlinear flexural-flexural-torsional dynamics of inextensional beams. I: equations of motion, *Journal of Structural Mechanics* 6 (4) (1978) 437–448.